Influence of ionic charge and dipole fluctuations on the lattice dynamics, dielectric properties, and infrared response of La_2CuO_4

Claus Falter and Frank Schnetgöke
Institut für Festkörpertheorie, Universität Münster, Wilhelm-Klemm-Strasse 10, 48149 Münster, Germany
(Received 26 February 2001; revised manuscript received 2 October 2001; published 8 January 2002)

We generalize our recently proposed microscopic formulation of the electronic density response and screening and apply it to lattice dynamics and, also to the dielectric properties of the high-temperature superconductors (HTSC's). Our previously developed method of screening in the HTSC in terms of ionic charge fluctuations (CF's) is extended by including additional dipole fluctuations as possible electronic polarization processes. The latter prove to be important in the HTSC, especially for the ions in the ionic layers. On the other hand, CF's are the dominating polarization process in the CuO planes. In particular, we have predicted in the past strong coupling via CF's of the high-frequency copper-oxygen bond-stretching modes in the HTSC. These modes are thought now to cause a kink in the electronic dispersion observed by photoemission. Our model calculations in this paper deal with both the metallic as well as the insulating phase of La_2CuO_4. Complete phonon dispersion curves are calculated for both phases and specific modes discussed controversially in the literature are studied in detail. Finally, the macroscopic high-frequency and static dielectric constants, transverse effective charges, and oscillator strengths of the infrared-active vibrations are investigated.

DOI: 10.1103/PhysRevB.65.054510 PACS number(s): 74.25.Kc, 63.20.Dj, 63.10.+a

I. INTRODUCTION

High-temperature superconductors (HTSC's) are materials displaying an anisotropic mixed ionic-covalent (metallic) bonding. While the ionic nature of bonding predominates along the *c* axis, covalent (metallic) bonding contributions become important in the CuO plane. In our microscopic modeling of the charge response in the HTSC the ionic nature is described by an *ab initio* rigid-ion model (RIM) leading to a local rigid charge response, while the nonlocal, nonrigid part of the electronic density response is modeled up to now parameter free by more or less localized charge fluctuations on the outer shells of the ions. In this procedure covalent metallic features of bonding in the HTSC are taken approximately into account by the electronic band structure: first, in a global way by using effective ionic charges in the RIM, as calculated from a tight-binding analysis of the (first-principles) electronic band structure, and second, via the electronic polarizability, which contains the kinetic one-particle part of the charge response (see Sec. II). The latter is also calculated from the electronic band structure.

There are many experimental observations of strong electron-phonon interactions (EPI) in the literature[1–6] that demonstrate that the electron-phonon mechanism is present in the HTSC and plays an important role. This point of view is supported also by theoretical studies; see, for example, Refs. 7–14. It is thus of great interest to investigate in detail the lattice dynamical properties of the HTSC and to analyze the type of electronic charge response excited by the vibrating ions that finally leads to the characteristic features in the phonon dispersion curves and to a strong EPI.

Interesting experimental evidence of a large and anomalous EPI, accompanied by corresponding phonon softening, is provided by inelastic neutron scattering in La_2CuO_4. Here a strong renormalization of phonon branches related to high-frequency copper–in-plane-oxygen bond-stretching modes is found as holes are doped in the insulating parent compound, i.e., there is a clear correlation of hole doping with the phonon anomalies. Our calculations[8–11] have revealed the type of charge response leading to the strong coupling and accordingly to these anomalies and demonstrated that the softening is driven by nonlocal electron-phonon interaction effects of ionic charge-fluctuation type. Recently, we have extended our calculations to $YBa_2Cu_3O_7$ (Ref. 14) and found that the same strong-coupling effects via ionic charge fluctuations as in La_2CuO_4 lead to the pronounced softening of the high-frequency copper–in-plane-oxygen bond-stretching modes experimentally observed also in this material.[1] In $YBa_2Cu_3O_7$ a doubling of the strongly coupling anomalous oxygen bond-stretching modes is obtained as compared to La_2CuO_4.

Very recently, direct evidence for the strong EPI has also been found experimentally by photoemission, causing a kink in the electronic dispersion.[5] The strong-coupling phonon modes responsible for this effect are thought to be just the high-frequency copper-oxygen bond-stretching modes predicted by our calculations.[8–11,14]

These results point to the importance of the nonlocal EPI of ionic charge-fluctuation type for the pairing mechanism in the HTSC. One should realize in this context that such a type of coupling, not present in conventional metals and superconductors, is a specific feature of the HTSC favoring a localized charge response in form of localized charge fluctuations (CF's). Note, however, that our theoretical method only deals with coupled lattice and charge degrees of freedom. Nothing can be said about the role of spin fluctuations or other possible mechanisms for Cooper pairing of the current carriers. In the literature the significance of nonphononic mechanisms is frequently brought into relation with the very weak isotopic effect observed in many HTSC materials.

In principle, a density response in terms of CF's can also be expected in classical ionic crystals, however, less marked

as compared to HTSC's because of their nearly closed ionic shells in contrast to the open-shell ions in the CuO plane. From the calculations in Ref. 13 it can be concluded that in classical ionic crystals electronic polarization effects of the dipole type (dipole fluctuations) govern the screening to a large extent. This, of course, can also be expected from the success of the phenomenological shell model in fitting phonon dispersion curves of ionic crystals. In case of the HTSC, besides the dominating screening effect mediated by the CF's in the CuO plane, the contribution of the dipole fluctuations (DF's) to the electronic density response can be expected to become important in particular for the ions in the ionic layers when vibrating in a polar mode.

Thus, we are left with interesting problems to be discussed in this work, namely, the calculation of the effect of the DF in addition to the CF on the phonon dispersion in the metallic and insulating phases and moreover, the investigation of the dielectric properties and the infrared response, which has never been done before on a microscopic basis to the best of our knowledge.

Another topic to be addressed in this work is the problem of a possible Peierls instability of the planar oxygen breathing mode in La_2CuO_4, which was predicted in other calculations, and the renormalization of the so-called quadrupolar mode associated in the literature with a Jahn-Teller electron-phonon interaction. Both statements are not supported by our calculations here.

From a general point of view our treatment of the electronic density response and lattice dynamics in terms of DF's and CF's can be considered as a microscopic (semi-*ab-initio*) implementation of the phenomenological dipole shell model or the charge-fluctuation models, respectively. For a general formulation of phenomenological models for lattice dynamics that use localized electronic variables as adiabatic degrees of freedom, see, for example, Ref. 15. This formulation covers shell models of all types, bond-charge models, and charge-fluctuation models. While in the latter approach the coupling coefficients are treated as fitting parameters, the essential point of our microscopic scheme is that it allows for a calculation of all the couplings appearing in the dynamical matrix, the dielectric properties, and the infrared response.

In the present paper we investigate for the HTSC the combined effect of CF and DF on the lattice dynamics, the dielectric properties, and the infrared response using La_2CuO_4 as an example. For this material the experimental information is most complete.[1,4,6,16–18] Concerning the DF's we expect an anisotropic form of the dipole polarizability of the ions because of the layered structure of the HTSC with alternating ionic layers and ionic-covalent CuO planes. The largest component of the dipole polarizability should be along the (ionic) *c* direction. The transverse components can be expected to vanish almost entirely in the CuO planes because of the covalent screening contribution and should in general be smaller than the corresponding *z* component along the *c* axis in the ionic layers. The calculation of the dipole polarizability in our approach is performed with the help of the Sternheimer method in the framework of density-functional theory (DFT) in the local-density approximation (LDA), taking self-interaction effects (SIC's) into account.[13,19,20] In this procedure effects of anisotropy of the dipole polarizability are not taken into account. Thus, we model this anisotropy by reducing the calculated polarizability in the transverse directions and the most likely form of the DF is singled out from a comparison of the calculated results of the phonon dispersion with the experimental data.

In Sec. II the theory and modeling are reviewed to provide a certain degree of self-consistency of the paper. Section III presents the calculations of the phonon dispersion of La_2CuO_4 and of the dielectric properties such as the high-frequency and static dielectric constants, transverse effective charges, and the oscillator strengths of the infrared-active modes taking CF's and DF's into account. Starting from an *ab initio* RIM that serves as a reference system for the description of the HTSC, we calculate and discuss in detail the effects of the ionic CF's and DF's on the phonon dispersion in the metallic and the insulating phase. The results are compared with experiments and other calculations in the field. In particular, we address the phonon anomalies driven by nonlocal EPI effects, and the anisotropy of screening due to dipole fluctuations, which are important for the optical A_{2u} and E_u modes. Section IV contains a summary and the conclusions.

II. THEORY AND MODELING

A detailed description of our microscopic approach of the electronic density response, the lattice dynamics, and the electron-phonon interaction in the HTSC can be found, for example, in Refs. 8 and 13. In this formulation the local part of the electronic charge response is approximated by an *ab initio* rigid-ion model taking into account ion softening in terms of effective ionic charges as calculated from a tight-binding analysis of the electronic band structure. In addition, scaling of the short-range part of the pair potentials between the ions is considered in order to simulate covalence effects in the calculations.[21] Scaling is performed in such a way that the energy-minimized structure is as close as possible to the experimental one. The tight-binding analysis supplies the effective ionic charges as extracted from the orbital occupation numbers Q_μ of the μ (tight-binding) orbital in question:

$$Q_\mu = \frac{2}{N} \sum_{n\mathbf{k}} |C_{\mu n}(\mathbf{k})|^2. \tag{1}$$

$C_{\mu n}(\mathbf{k})$ stands for the μ component of the eigenvector of band n at wave vector $\mathbf{k}$ in the first Brillouin zone; the summation in Eq. (1) runs over all occupied states and N gives the number of elementary cells in the (periodic) crystal. The rigid-ion model with the corrections just mentioned then serves as a reference system for the description of the HTSC. For a representation of the (nonrigid) electronic density response and screening in the HTSC, particularly in the metallic phase, more or less localized electronic charge fluctuations in the outer shells of the ions are considered. The latter dominate the long-ranged, nonlocal contribution of the electronic density response and the EPI in the HTSC. In addition, dipole fluctuations can be treated within our approach.[13]

Thus, the starting point of our model is the ionic density in the perturbed state, which is given by

$$\rho_\alpha(\mathbf{r}) = \rho_\alpha^0(r) + \sum_\lambda Q_\lambda \rho_\lambda^{\mathrm{CF}}(r) + \mathbf{p}_\alpha \cdot \hat{\mathbf{r}} \rho_\alpha^D(r). \tag{2}$$

ρ_α^0 is the density of the unperturbed ion localized at the sublattice α of the crystal. Q_λ and $\rho_\lambda^{\mathrm{CF}}$ describe the amplitudes and the form factors of the charge fluctuations and the last term in Eq. (2) gives the dipolar deformation of an ion α with amplitude (dipole moment) $\mathbf{p}_\alpha$ and a radial density distribution ρ_α^D. $\hat{\mathbf{r}}$ is the unit vector in the direction of $\mathbf{r}$. $\rho_\lambda^{\mathrm{CF}}$ are approximated by a spherical average of the orbital densities of the outer ionic shells calculated in local-density approximation taking self-interaction effects into account. The dipole density ρ_α^D is obtained from a modified Sternheimer method in the framework of LDA SIC; see Refs. 13, 19, and 20.

The total energy of the crystal is investigated by assuming that the density of the crystal can be approximated by a superposition of overlapping densities of the individual ions ρ_α. The ρ_α^0 are calculated within LDA SIC taking environment effects via a Watson sphere potential and calculated effective charges of the ions into account. Such an approximation holds well for HTSC's.[21,22] Moreover, applying the pair-potential approximation we get for the total energy

$$E(R,\zeta) = \sum_{\mathbf{a}\alpha} E_\alpha^{\mathbf{a}}(\zeta) + \tfrac{1}{2} {\sum_{\substack{\mathbf{a}\alpha \\ \mathbf{b}\beta}}}' \phi_{\alpha\beta}(\mathbf{R}_\beta^{\mathbf{b}} - \mathbf{R}_\alpha^{\mathbf{a}}, \zeta). \tag{3}$$

The energy E depends on the configuration of the ions $\{R\}$ and the electronic degrees of freedom (EDF) $\{\zeta\}$ of the charge density, i.e., $\{Q_\lambda\}$ and $\{\mathbf{p}_\alpha\}$ in Eq. (2). $E_\alpha^{\mathbf{a}}$ are the energies of the single ions. **a** and **b** denote the elementary cells in the crystal and α and β the sublattices. The second term in Eq. (3) is the interaction energy of the system, expressed by the pair interactions $\phi_{\alpha\beta}$. The prime in Eq. (3) means that the self-term has to be omitted. Both $E_\alpha^{\mathbf{a}}$ and $\phi_{\alpha\beta}$ in general depend upon ζ via ρ_α.

From the adiabatic condition

$$\frac{\partial E(R,\zeta)}{\partial \zeta} = 0, \tag{4}$$

an expression for the force constants, and accordingly, the dynamical matrix in harmonic approximation can be derived:

$$t_{ij}^{\alpha\beta}(\mathbf{q}) = [t_{ij}^{\alpha\beta}(\mathbf{q})]_{\mathrm{RIM}} - \frac{1}{\sqrt{M_\alpha M_\beta}} \times \sum_{\kappa,\kappa'} [B_i^{\kappa\alpha}(\mathbf{q})]^* [C^{-1}(\mathbf{q})]_{\kappa\kappa'} B_j^{\kappa'\beta}(\mathbf{q}). \tag{5}$$

$[t_{ij}^{\alpha\beta}(\mathbf{q})]_{\mathrm{RIM}}$ denotes the contribution of the RIM to the dynamical matrix. M_α and M_β are the masses of the ions and $\mathbf{q}$ is a wave vector from the first Brillouin zone. The quantities $\mathbf{B}(\mathbf{q})$ and $C(\mathbf{q})$ represent the Fourier transforms of the coupling coefficients as calculated from the energy,

$$\mathbf{B}_{\kappa\beta}^{\mathbf{ab}} = \frac{\partial^2 E(R,\zeta)}{\partial \zeta_\kappa^{\mathbf{a}} \partial \mathbf{R}_\beta^{\mathbf{b}}}, \tag{6}$$

and

$$C_{\kappa\kappa'}^{\mathbf{ab}} = \frac{\partial^2 E(R,\zeta)}{\partial \zeta_\kappa^{\mathbf{a}} \partial \zeta_{\kappa'}^{\mathbf{b}}}. \tag{7}$$

The derivatives in Eqs. (6) and (7) must be performed at the equilibrium positions. κ denotes the electronic degrees of freedom (charge fluctuations and dipole fluctuations in the present model) in an elementary cell of the crystal. The **B** coefficients describe the coupling between the EDF and the ions and the C coefficients the interaction between the EDF. Equations (5)–(7) are generally valid and, in particular, are independent of our specific model for the decomposition of the perturbed density in Eq. (2) and of the pair approximation (3) for the energy.

The pair interactions $\phi_{\alpha\beta}$ can be decomposed into long-range Coulomb contributions and short-ranged terms. The latter are separated into the interaction between the ion cores and the charge density from Eq. (2), the interaction between the density ρ_α and the density ρ_β (Hartree contribution), and a term representing the sum of the kinetic one-particle and the exchange-correlation contribution of the interaction between the two ions. A detailed description of the $\phi_{\alpha\beta}$ and the calculation of the coupling coefficients **B** and C for the EDF is given in Ref. 13. In this context it should be mentioned that the matrix $C_{\kappa\kappa'}(\mathbf{q})$ of the EDF-EDF interaction, whose inverse appears in Eq. (5), for the dynamical matrix can also be written as

$$C = \Pi^{-1} + \tilde{V}. \tag{8}$$

Π^{-1} contains the kinetic one-particle part of the interaction and $\tilde{V}$ the Hartree and exchange-correlation contribution. The quantity C^{-1} needed for the calculation of the dynamical matrix is closely related to the density response function (matrix) and to the inverse dielectric function (matrix) ε^{-1}. Written in matrix notation we have the relation

$$C^{-1} = \Pi(1 + \tilde{V}\Pi)^{-1} \equiv \Pi \varepsilon^{-1}, \quad \varepsilon = 1 + \tilde{V}\Pi. \tag{9}$$

The CF-CF submatrix of the matrix Π can be calculated approximatively from a tight-binding analysis of the (first-principles) electronic band structure. In this case the electronic polarizability Π is given by

$$\Pi_{\kappa\kappa'}(\mathbf{q}) = -\frac{2}{N} \sum_{\substack{n,n' \\ \mathbf{k}}} \frac{f_{n'}(\mathbf{k}+\mathbf{q}) - f_n(\mathbf{k})}{E_{n'}(\mathbf{k}+\mathbf{q}) - E_n(\mathbf{k})} \times [C_{\kappa n}^*(\mathbf{k}) C_{\kappa n'}(\mathbf{k}+\mathbf{q})][C_{\kappa' n}^*(\mathbf{k}) C_{\kappa' n'}(\mathbf{k}+\mathbf{q})]^*. \tag{10}$$

f, E, and C are the occupation numbers, the electronic band structure, and the expansion coefficients of the Bloch functions in terms of the tight-binding functions.

Within the framework of our theoretical description of the electronic density response we can derive expressions for the

macroscopic high-frequency dielectric constant $\varepsilon_\infty(\hat{\mathbf{q}})$ and the transverse effective charges Z_α^T. For $\varepsilon_\infty(\hat{\mathbf{q}})$, $\hat{\mathbf{q}}=\mathbf{q}/q$ we get[23]

$$\varepsilon_\infty(\hat{\mathbf{q}}) = \lim_{\mathbf{q}\to 0} 1/[1-v(q)\chi_0(\mathbf{q})], \tag{11}$$

with

$$v(q) = \frac{4\pi}{V_z q^2}, \tag{12}$$

and

$$\chi_0(\mathbf{q}) = \sum_{\kappa,\kappa'} \rho_\kappa(\mathbf{q})[C^{-1}(\mathbf{q})]_{\kappa\kappa'}\rho^*_{\kappa'}(\mathbf{q}). \tag{13}$$

V_z denotes the volume of the elementary cell and $\rho_\kappa(\mathbf{q})$ is the Fourier transform of $\rho_\lambda^{\mathrm{CF}}(r)$ (charge fluctuation) and $\hat{\mathbf{r}}\rho_\alpha^D(\mathbf{r})$ (dipole fluctuation).

The transverse effective charges can be extracted in the limit $\mathbf{q}\to\mathbf{0}$ from the equation

$$\hat{\mathbf{q}}\underline{Z}_\alpha^T\hat{\mathbf{q}} = \lim_{\mathbf{q}\to\mathbf{0}}\left\{\varepsilon_\infty(\hat{\mathbf{q}})\left[Z_\alpha + i\frac{\mathbf{q}}{q^2}\left(\sum_\kappa \rho_\kappa(\mathbf{q})\mathbf{X}^{\kappa\alpha}(\mathbf{q})\right)\right]\right\}. \tag{14}$$

Here $\underline{Z}_\alpha^T$ is the transverse effective-charge tensor, which is diagonal for tetragonal symmetry with two independent components. The latter can be calculated from Eq. (14) by using $\hat{\mathbf{q}}\perp c$ and $\hat{\mathbf{q}}\| c$. The quantity $\mathbf{X}^{\kappa\alpha}(\mathbf{q})$ describes the self-consistent response of the EDF when a perturbation is applied and can be shown to be given (in formal matrix notation) by

$$\mathbf{X}(\mathbf{q}) = C^{-1}(\mathbf{q})\mathbf{B}(\mathbf{q}) = \Pi(\mathbf{q})\varepsilon^{-1}(\mathbf{q})\mathbf{B}(\mathbf{q}). \tag{15}$$

III. LATTICE DYNAMICS, DIELECTRIC PROPERTIES, AND INFRARED RESPONSE OF La_2CuO_4

A. The ionic reference system and the experimental dispersion

For a definitive discussion of the phonon renormalization induced by the nonlocal EPI effects of the ionic CF and DF types, mediated by the second term in the dynamical matrix from Eq. (5), a quantitative reference model for the calculation of the phonon dispersion based exclusively on the ionic component of binding is necessary. Such a model, representing approximately the local EPI effects, is provided by the *ab initio* rigid-ion model sketched in Sec. II.

In the following, two versions of rigid-ion models R1 and R2 are considered. In both models ion softening as calculated from a tight-binding analysis of the electronic band structure is taken into account, leading to effective ionic charges. According to Ref. 21 we obtain the following results: $Cu^{1.22+}$, $O_{xy}{}^{1.42-}$, $O_z{}^{1.47-}$, $La^{2.28+}$. In model R2, in addition to model R1, scaling of the short-range part of the Cu-O_{xy}, O_{xy}-La, and O_z-La pair potential is performed. The corresponding outcome for the structural parameters in the two models as obtained from an energy minimization is given in Table I. Without scaling, i.e., in model R1, the planar lattice constant a is overestimated and c is underestimated while the internal positions of O_z and La are well described. Taking scaling into account as in model R2 it is possible to find a solution that is in excellent agreement with the experimental crystal structure.[24]

TABLE I. Structural parameters of tetragonal La_2CuO_4 for the two rigid-ion models R1 and R2 as defined in the text together with the experimental data. The lattice constants a and c are given in Å and the internal positions of the apex oxygen O_z and the La atom are in units of c. The experimental data are from Ref. 24.

	a	c	$Z(O_z)$	Z(La)
R1	4.134	12.682	0.1879	0.1333
R2	3.784	13.224	0.1846	0.1337
Expt.	3.790	13.227	0.1820	0.1380

In Fig. 1 the calculated phonon dispersion of La_2CuO_4 in the main symmetry directions $\Delta\sim(1,0,0)$, $\Sigma\sim(1,1,0)$, and $\Lambda\sim(0,0,1)$ as calculated with model R1 is compared with the experiments for the insulating phase.[1,3,16] The width of the spectrum already agrees quite well with the experimental data. This is mainly due to ion softening, i.e., a global covalence effect, expressed by the effective ionic charges in model R1. This can be extracted from the fact that the oxygen breathing mode at the X point, O_B^X (in O_B^X essentially the planar oxygens vibrate in phase along the CuO bonds), which is the highest mode in the spectrum (end point of the highest Σ_1 branch; for the notation see the figure caption of Fig. 1), decreases from 33.35 THz in a model using nominal ionic charges,[21] i.e., Cu^{2+}, O^{2-}, La^{3+}, to 25.82 THz in model R1. Moreover, some of the branches that are unstable in the model with nominal charges are stabilized in model R1, while a few typical branches remain unstable.

In model R1 the unstable modes at Γ are the lowest E_g (-1.88 THz) and E_u modes ($E_u^L=-1.74$ THz, longitudinal optic mode; $E_u^T=-4.89$ THz, transverse optic mode). Note that imaginary frequencies are represented here by negative numbers. These modes are characterized essentially by displacements of the apex oxygens, O_z, and the La atoms parallel to the CuO plane (sliding modes). In first-principles density-functional calculations within the LDA these modes are also found to be soft or unstable, respectively,[25,26] and are shown by frozen phonon calculations to display anharmonic energy versus displacement relationships.[25,27]

Unstable modes at X are again two O_z-La sliding modes ($B_{2u}=-4.92$ THz, $B_{3u}=-1.49$ THz), the tilt mode ($B_{2g}=-6.42$ THz), which involves a rotation of the CuO_6 octahedra along the $(1,-1,0)$ direction and two other rotation modes of the octahedra: one around the c axis ($B_{1g}=-7.16$ THz) and another one along the (1,1,0) direction ($B_{3g}=-3.02$ THz). The instability of these modes is a consequence of the purely ionic nature of the forces in the model together with the assumed tetragonal symmetry of the structure.

Figure 2 shows the calculated results of the phonon dispersion in model R2 taking scaling (predominantly of the Cu-O bond in the plane) into account. Comparing with Fig. 1 we find a considerable improvement of the phonon disper-

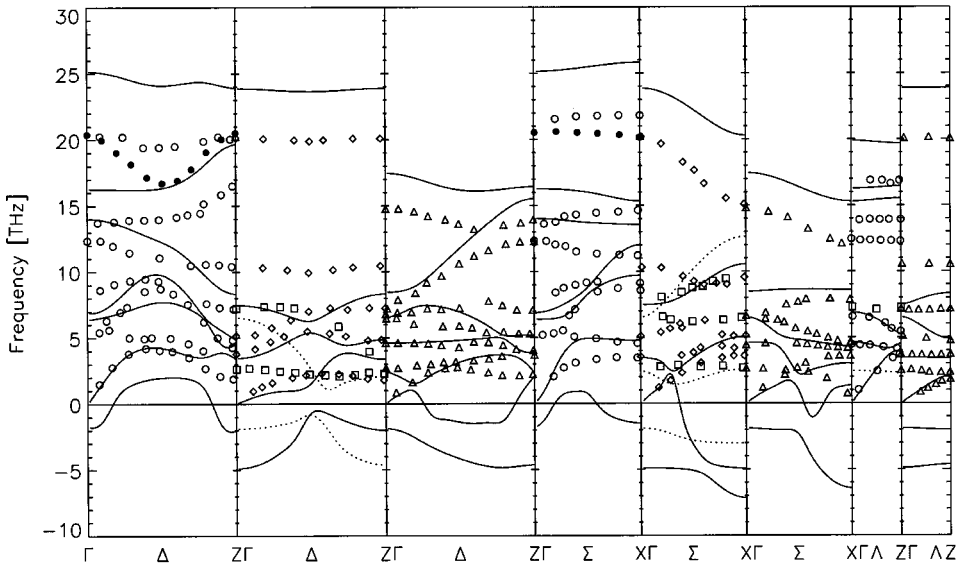

FIG. 1. Calculated phonon dispersion of (tetragonal) La_2CuO_4 in the main symmetry directions $\Delta\sim(1,0,0)$, $\Sigma\sim(1,1,0)$, and $\Lambda\sim(0,0,1)$ as calculated for the rigid-ion model R1 explained in the text. The experimental data are taken from Refs. 1, 3, and 16. The various open symbols representing the experimental results for the insulating phase indicate different irreducible representations (ID). The arrangement of the panels from left to right is as follows: Δ_1; (Δ_2,$\cdots$; Δ_4,—); Δ_3; Σ_1; (Σ_2,$\cdots$; Σ_4,—); Σ_3; (Λ_1,—; Λ_2,$\cdots$); Λ_3. The solid circles represent the experimental values of the highest Δ_1 and Σ_1 branches for the optimally doped, metallic phase $La_{1.85}Sr_{0.15}CuO_4$. As compared with the notation used in the experiments for the classifying ID's the following changes should be noted: $\Delta_3\leftrightarrow\Delta_4$, $\Sigma_3\leftrightarrow\Sigma_4$, $\Lambda_3\leftrightarrow\Lambda_5$. The frequencies are in THz and the imaginary frequencies are represented as negative numbers.

sion for various single branches, for example, the (*xy*)-polarized Λ_3 modes, as well as for the width of the spectrum, which is reduced by about 2 THz ($O_B^X = 23.95$ THz). In particular, all the unstable branches have disappeared except the branch with the tilt mode at *X*. Freezing in of this distortion points correctly to the experimentally observed structural phase transition from the tetragonal to the low-temperature orthorhombic (LTO) structure. The actual transition, of course, cannot be described in the harmonic approximation because the anharmonic energy must be taken into account.[25,27] The anharmonicity of the lattice near the structural phase transition also manifests itself in the anomalous behavior of the oxygen and copper isotopic effects.[28,29]

Next we will discuss some typical modes not well represented in the RIM. The so-called scissor mode (end point of the second highest Σ_1 branch at the *X* point), where the in-plane oxygens vibrate perpendicular to the Cu-O bonds is seriously overestimated in frequency in model R2 ($A_g^{sc} = 19.12$ THz) as compared with experiment [$A_g^{sc} = 14.7$ THz (Ref. 16)]. As the reason for this high frequency we identify the large contribution from the long-ranged Coulomb interactions. A calculation ignoring the short-ranged part of the pair interactions already leads to 13.88 THz, which is the highest frequency at the *X* point in a calculation where only long-ranged Coulomb interactions are considered. For such a bond-bending vibration like the scissor mode it can be ex-

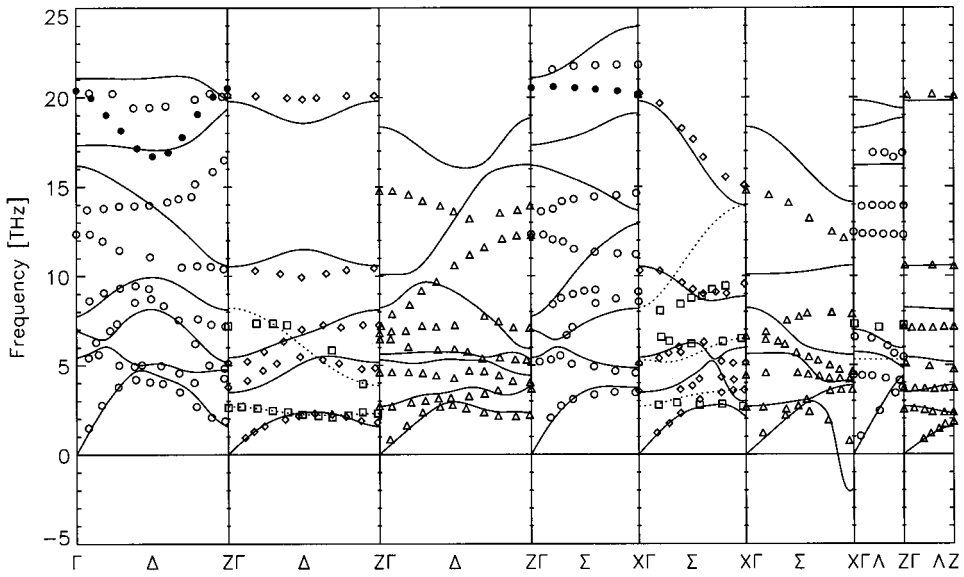

FIG. 2. Same as Fig. 1 with the calculated results taken from the rigid-ion model R2 (see the text) taking scaling into account.

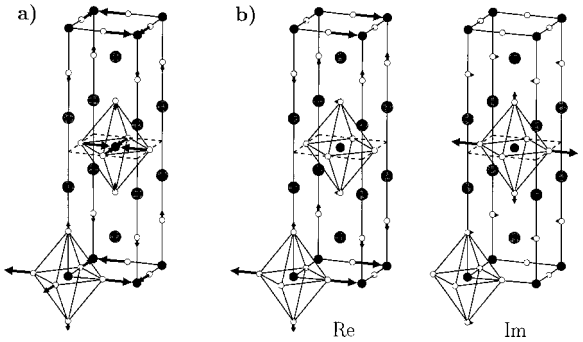

FIG. 3. Displacement patterns of the high-frequency Cu–in-plane-oxygen bond-stretching modes of La_2CuO_4 (a) for O_B^X and (b) for the $\Delta_1/2$ minimum. In case of $\Delta_1/2$ the real part (Re) and the imaginary part (Im) are shown.

pected that specific covalent bonding contributions are important. Our calculations in Secs. III B and III C have shown that the scissor mode is virtually not influenced by CF on the ions and DF's lead only to a modest decrease of the frequency by less than 1 THz. Thus, in order to improve the agreement selectively for this mode we propose in Sec. III B a model, where, in addition to the calculated ionic CF's, off-site CF's are installed empirically to simulate the missing covalency.

In contrast to the scissor mode the high-frequency Cu–in-plane-oxygen bond-stretching modes including the breathing mode O_B^X and especially the highest Δ_1 branch are strongly renormalized in the metallic phase by ionic CF's generated through nonlocal EPI effects as has been shown in Refs. 8, 10, 11, and 14 and is also evident from the investigations in Sec. III B. From experiments there is a clear correlation of hole doping with the strong softening of these modes in the metallic phase as can be extracted from Figs. 1 and 2. Here the solid circles represent the experimental data of these phonons in the optimally doped metallic phase and the open circles in the insulating phase. Thus, the enhancement of the ionic CF's produced by a strong nonlocal EPI is very important for the doped metallic phase and consequently an important ingredient of the pairing mechanism in HTSC's. A description of pairing via a nonlocal EPI can be found in Ref. 9. It leads to an interpretation of the experimentally observed universal relationship between T_c and the hole content in HTSC's. The importance of the Cu-oxygen bond-stretching modes is emphasized by the fact that the phase space for strong coupling by these modes has been shown to be large.[14] As representatives for the strong-coupling modes in Fig. 3 the displacement pattern of O_B^X and of the mode related to the minimum of the highest Δ_1 branch, called the $\Delta_1/2$ anomaly, is displayed.

As already mentioned in the Introduction, there is now also direct evidence for a strong coupling of these modes to the electrons leading to a kink in the electronic dispersion, as observed by photoemission in Ref. 5. According to a calculation in Ref. 30 a very strong renormalization of O_B^X leading ultimately to a Peierls instability of the lattice has been predicted, which, however, is not found in the experiments where this mode appears as the highest mode in the spectrum (see Figs. 1 and 2). Fermi-surface nesting effects leading to gigantic Kohn anomalies that have been proposed to be the reason for the strong softening can be ruled out because the enhancement found in Ref. 30 for the intraband contribution of the scalar polarizability [which can be obtained from the full polarizability in Eq. (10) equating $C_{\kappa n}$ to 1] is strongly suppressed if the eigenvectors $C_{\kappa n}$ are taken into account.[14] On the other hand, the calculated behavior found in models R1 and R2 and in our earlier results[8] is consistent with experiment. The reason for the high frequency of O_B^X is found by our calculation to be related to the fact that the long-ranged Coulomb interaction between the ions alone already leads to a frequency of 11.42 THz for O_B^X. The missing contribution from the short-ranged part of the pair interactions further stabilizes this mode to its actual high value.

In contrast to O_B^X and the scissor mode the so-called quadrupolar mode leading to a rhombic distortion of the oxygen squares around the Cu ions is strongly destabilized by the long-ranged Coulomb interactions ($B_{1g}^Q = -12.53$ THz). It is the most unstable mode at X for the case when short-range contributions of the interaction are ignored. Taking the latter into account, we learn from Fig. 2 that the highest Σ_4 branch with the quadrupolar mode as its end point is already well described by the ionic reference model R2, i.e., by the ionic forces alone. For symmetry reasons there are no ionic CF's. The fluctuations add up destructively in this mode. So we conclude that a quadrupolar deformation of the octahedra is very much promoted by the long-range Coulomb interactions. A phonon renormalization due to a Jahn-Teller electron-phonon interaction as proposed in Ref. 31 is unlikely and is at most of minor importance. The quadrupolar mode and the scissor mode are virtually uninfluenced by doping.[16]

Finally, we would like to comment on the modes propagating in the Λ direction, i.e., along the c axis. The doubly degenerate Λ_3 modes (E_g and E_u at the Γ point) polarized parallel to the xy plane are well described by the ionic reference model (see Fig. 2). On the other hand, in the case of the Λ_1 modes, which are polarized along the c axis, a considerable renormalization is required. It will be shown in Sec. III C that the main screening effects for these modes are due to anisotropic dipole fluctuations with a dominating z component along the ionic c axis of the HTSC.

B. Phonon dispersion in the metallic phase: On-site and off-site charge fluctuations and dipole fluctuations

As far as underdoped and even optimally doped La_2CuO_4 is concerned the optical infrared c-axis spectra display the typical features of an insulator. They are dominated by optical A_{2u} phonons and are almost unchanged from the insulator upon doping.[17,32,33] As discussed in Ref. 12 a typical LDA-like band structure taken as input for the calculation of the electronic polarizability is not able to describe the strong anisotropy of the charge response in the c direction seen in the experiments. In this investigation the electronic band structure was taken from a tight-binding representation of the first-principles band structure given in Ref. 34 including La $5d$; Cu $3d,4s,4p$; and O $2p$ states leading to a 31-band

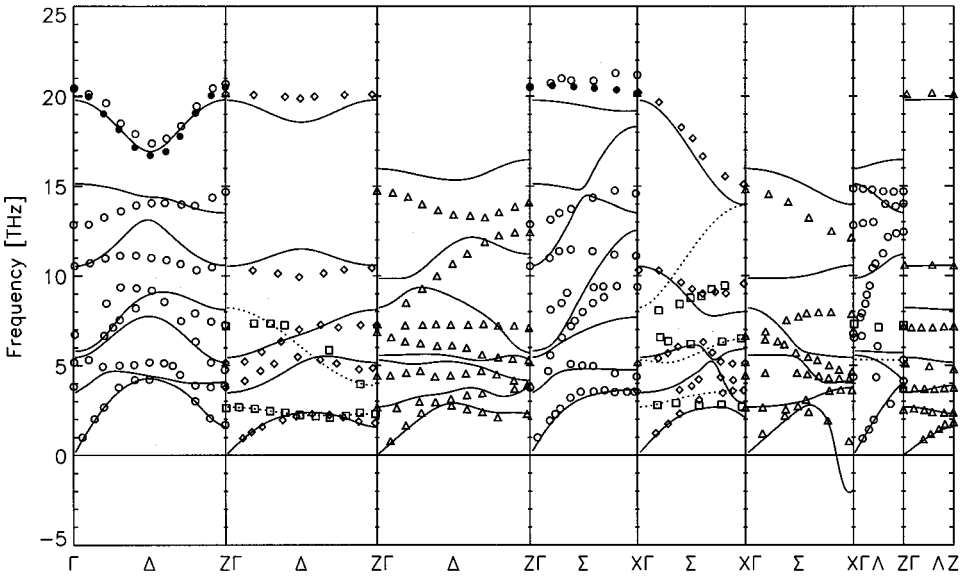

FIG. 4. Calculated phonon dispersion for the metallic phase of tetragonal La_2CuO_4. The experimental values for this phase ($La_{1.9}Sr_{0.1}CuO_4$), represented by various symbols as in Fig. 1, are taken from Refs. 1, 3, and 16. The notation for the irreducible representations and the arrangement of the panels is the same as in Fig. 1. The calculations are based on the model M1 as defined in the text.

model (31 BM). The effective ionic charges used in model R1 and R2 are consistent with this model.

It is well known that the insulating phase of the HTSC and in particular the phonons in this phase cannot be described rigorously with a DFT LDA calculation because LDA predicts a metallic state for these materials. Moreover, in Ref. 12 it has been shown that even in the metallic, optimally doped probe of the HTSC's, calculations that rely on the adiabatic approximation, i.e., static screening, only apply outside a small conelike region around the *c* axis (Λ direction). The charge response inside the cone is nonadiabatic and similar to that of an ionic insulator as seen in the optical experiments. The transition from such an insulatorlike charge response to a metallic, adiabatic charge response outside the cone has been explained in Ref. 12. In this context also a possible solution has been provided why, in contrast to the optical experiments, neutron scattering[1,16] predicts along the $\Lambda \sim (0,0,1)$ direction a phonon dispersion that is typical for a three-dimensional anisotropic metal as calculated in the adiabatic approximation. Here, different from the optical results, the discontinuities of the A_{2u} modes appear to be closed, and simultaneously, a characteristic Λ_1 branch with a steep dispersion appears in the spectrum (see, for example, the corresponding data points in Fig. 4).

Following the considerations in Ref. 12 this observed typical adiabatic behavior can be explained by the fact that the wave vector in the *c* direction cannot be fixed with a sufficiently high precision in the experiments. In such a situation the small region of nonadiabatic insulatorlike charge response around the Λ direction is overbalanced by a significantly larger part (within which the wave vector will be scattered) where the charge response and the phonon dispersion are adiabatic.

An adiabatic calculation based on the 31 BM has been performed in Ref. 35, which, however, only qualitatively displays the characteristic Λ_1 branch. The dispersion is by far not so steep as in the experiments. In Fig. 4 we have repeated a calculation in the adiabatic approximation using a simpler model for the polarizability matrix from Eq. (10). This model has been derived from the 31 BM, taking into account diagonal matrix elements only.[11] With such a model (M1) we obtain phonon dispersion curves, which are in good agreement with those as obtained from the complete polarizability matrix of the 31 BM. We find that the Λ_1 branch with steep dispersion is only qualitatively represented as in the 31 BM. Otherwise the overall agreement of the calculated dispersion curves with experiment is quite good. In particular, the anomalous softening of the high-frequency Cu–in-plane-oxygen bond-stretching vibrations (full circles in Fig. 4) induced by the ionic CF's through the nonlocal EPI in the metallic phase is well described.

The relatively flat dispersion of the characteristic Λ_1 branch originates from the fact that the LDA-based results from the 31 BM or M1 overestimate the coupling along the *c* axis and underestimate the anisotropy. A strictly two-dimensional electronic structure results in a much better modeling of the charge response along the *c* axis. This can be achieved by neglecting in model M1 the CF's at La and the apex oxygen, O_z. This defines a strictly two-dimensional model where only Cu $3d,4s,4p$ and O_{xy} $2p$ CF's in the CuO plane are allowed. In the resulting phonon dispersion a much better representation of the steep Λ_1 branch is obtained. Note that at this stage of the modeling only ionic CF's derived from the 31 BM and no DF's are considered. In order to improve the scissor mode selectively, we additionally introduce empirically off-site CF's at the centers of the planar oxygen squares simulating covalence effects.

Now we come to the investigation of the influence of DF's in addition to CF's on the lattice dynamics of La_2CuO_4. As already noted in the Introduction the dipole polarizability in HTSC's should be very anisotropic with a dominating *z* component parallel to the ionic *c* direction and virtually no (*xy*) components in the CuO plane. Such a picture is confirmed by our calculation of the phonon dispersion in Fig. 5. In this calculation the two-dimensional model including off-site CF's is extended allowing for DF's only in the *c* direction on all ions in the elementary cell (model M2). The dipole polarizability of the ions has been calculated by

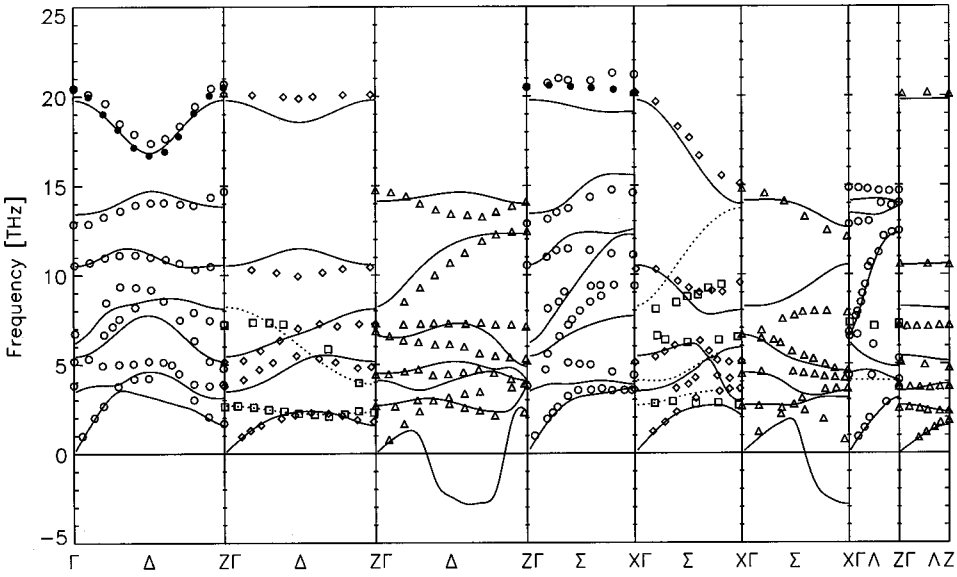

FIG. 5. Same as Fig. 4 with the calculated results as obtained from model M2.

the Sternheimer method in the framework of DFT LDA including SIC effects. Comparing the calculation of the dispersion in model M2 with that in M1 we find a considerable improvement for all phonon branches where *z* DF's are allowed (Δ_2, Δ_4, and Λ_3 do not couple to *z* DF's). In particular, the characteristic Λ_1 branch is now in excellent agreement with the experimental data.

Besides the tilt mode, in model M2 now another branch becomes unstable, namely, the lowest Δ_3 branch halfway in the Δ direction. The origin for this behavior is essentially related to the too large (calculated) dipole polarizability of the La ion. Nevertheless, the calculation demonstrates the sensitivity of the tetragonal structure against tilting along different tilt axes (compare with the discussion in Sec. III A). In the unstable Δ_3 mode the CuO_6 octahedra are locally tilted along the *y* axis, and this looks like a low-temperature tetragonal (LTT) structure that has been observed in the Ba-substituted material $La_{2-x}Ba_xCuO_4$ near $x=0.12$, where the superconductivity is drastically suppressed.[36] Note in this context that the calculated Ba^{2+} dipole polarizability is greater than that of La^{3+}, which would further enhance an instability of the type seen in the Δ_3 mode in case the Ba content is increased. Thus, in the model M2 we find a mixture of LTO and LTT local tilt directions corresponding to unstable mode behavior. Reducing the calculated La polarizability leads to a stabilization of the lowest Δ_3 branch.

Calculations assuming even only small (*xy*) components of the dipole polarizability for the atoms in the CuO plane results in a considerable softening of the (*xy*)-polarized phonon modes with the largest frequencies in the spectrum, like the E_u modes at Γ and O_B^X at the *X* point. Consequently the width of the spectrum decreases rapidly in disagreement with experiment. In addition, besides the tilt mode, the rotation mode of the planar oxygens around the *c* axis (B_{1g}) becomes unstable. So we conclude that to a good approximation the transverse components of the dipole polarizability can be

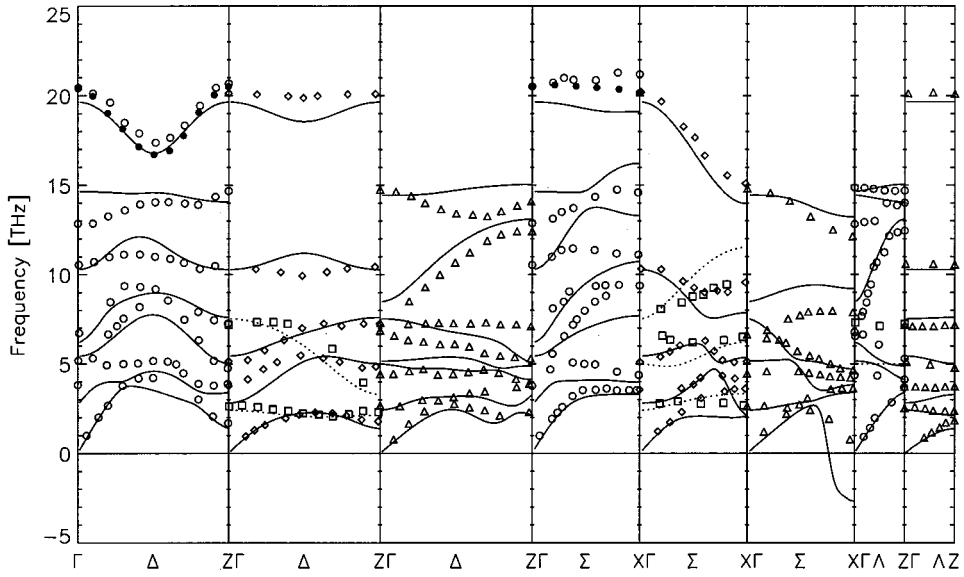

FIG. 6. Same as Fig. 4 with the calculated results as obtained from model M3.

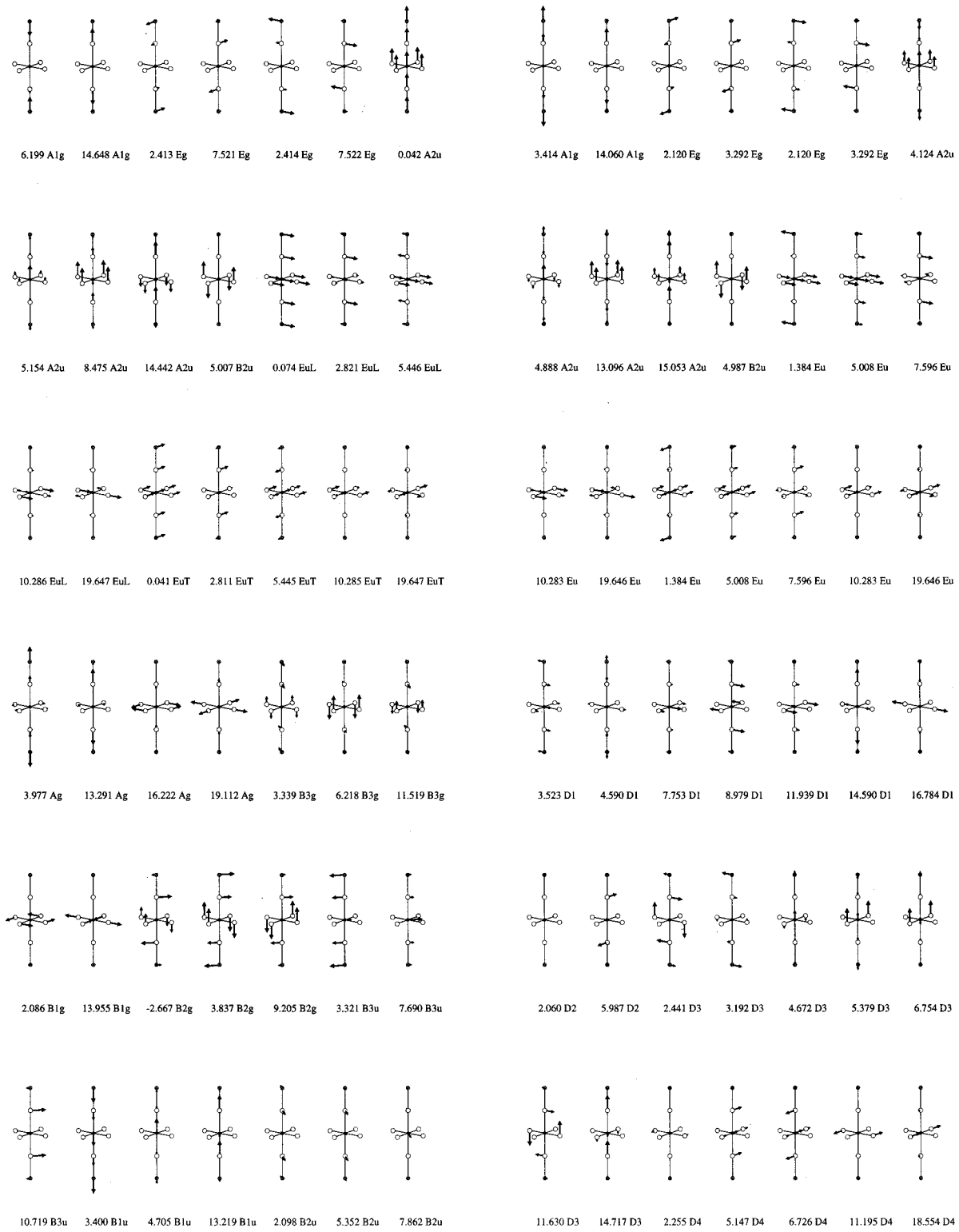

FIG. 7. Displacement patterns of the phonon modes for tetragonal La_2CuO_4 as calculated with model M3 at the symmetry points (from upper left to lower right) Γ, $Z=(0,0,2\pi/c)$, $X=(\pi/a,\pi/a,0)$, and $\Delta/2=(\pi/a,0,0)$. The frequencies are in units of THz. The data at the Γ point are calculated for numerical reasons for a small wave vector from the Δ direction, $(\zeta,0,0)(2\pi/a)$, $\zeta=0.005$. In case of the $\Delta/2$ point only the real part is shown.

neglected for the copper and the oxygen ions in the CuO plane.

Finally, in Fig. 6 we present a calculation with partially reduced dipole polarizabilities at the ions, model M3. A set of displacement vectors at the symmetry points Γ, Z, X, and $\Delta/2$ for this model is shown in Fig. 7. The lowest Δ_3 mode, being unstable in model M2, is stabilized in model M3 to 2.44 THz (see Figs. 6 and 7). Compared with the calculated

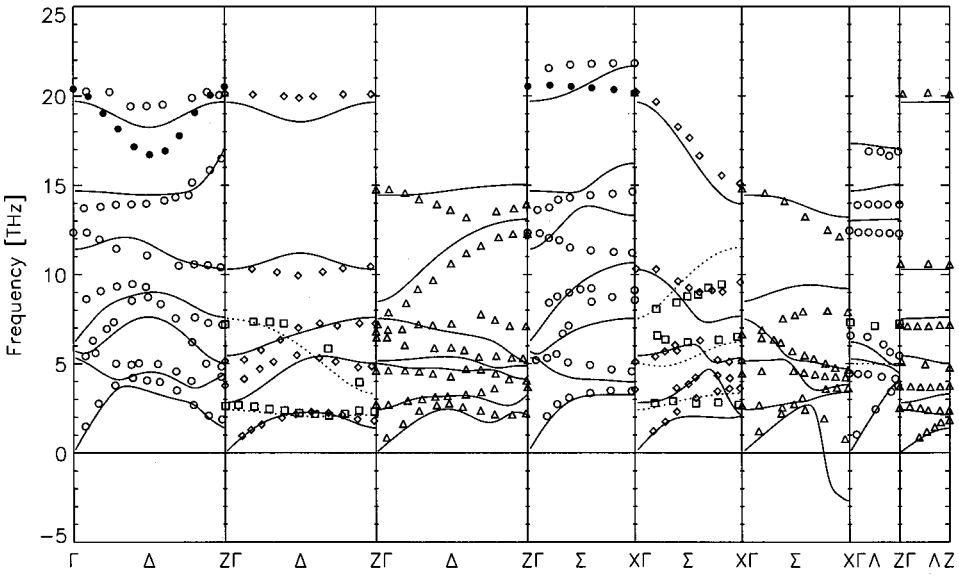

FIG. 8. Calculated phonon dispersion for the insulating phase of tetragonal La_2CuO_4. Experimental data and notation as in Fig. 1. The calculations are based on model I explained in the text.

values from the Sternheimer method that are normalized by definition to 100%, the following set of anisotropic polarizabilities has been used in model M3:

$$\mathrm{Cu}(z)=100\%, \quad \mathrm{Cu}(x,y)=0\%,$$

$$\mathrm{O}_{xy}(z)=30\%,$$

$$\mathrm{O}_{xy}(x,y)=0\%,$$

$$\mathrm{O}_z(z)=100\%, \quad \mathrm{O}_z(x,y)=40\%,$$

$$\mathrm{La}(z)=30\%,$$

$$\mathrm{La}(x,y)=40\%.$$

From a comparison of Figs. 5 and 6 with Fig. 4 it can be concluded that anisotropic DF's with a dominating z component are of importance for the screening processes in La_2CuO_4 as a prototype HTSC, in particular, for the infrared-active A_{2u} modes polarized along the c axis.

C. Phonon dispersion in the insulating phase: Infrared-active modes

For a description of the polarizability in the insulating phase of La_2CuO_4 that cannot be performed within DFT LDA we follow the procedure as proposed in Ref. 11. Here, the charge response is determined by requiring the fulfillment of rigorous sum rules for the density response in the long-wavelength limit. For an insulator, for example, the following sum rule for the polarizability matrix holds:

$$\sum_{\kappa'} \pi_{\kappa\kappa'}(\mathbf{q})=O(q), \tag{16}$$

$$\sum_{\kappa\kappa'} \pi_{\kappa\kappa'}(\mathbf{q})=O(q)^2, \tag{17}$$

as $\mathbf{q}\rightarrow\mathbf{0}$. On-site CF's are allowed in the CuO plane (Cu $3d$, O_{xy} $2p$) and off-site fluctuations at the center of the planar oxygen squares such that the sum rules hold. For details of the modeling see Ref. 11. As far as the DF's are concerned we consider a model for the anisotropy of the dipole polarizability that parallels model M3 for the metallic phase. The outcome for the phonon dispersion of this model (I) is shown in Fig. 8, and there is good agreement with experimental data. In particular, the longitudinal and transverse optical modes of A_{2u} and E_u symmetry are well described, including the screening contribution via anisotropic DF's. This can be seen by comparing Fig. 8 with the calculation within the RIM (R2 in Fig. 2).

In the last topic of this section we look at the infrared-active optical modes of La_2CuO_4 in more detail. For the A_{2u} modes polarized along the c axis a consensus about the eigenvectors and the assignment of the modes has not been reached.[17,37] In Table II the experimentally observed TO frequencies of the three possible infrared-active A_{2u} modes from several sources are collected together with our calculated results from model I. The latter compare well with the experiments, which themselves display some scattering. For other theoretical calculations and for the eigenvectors see also Table III. The oscillator strength of the lowest mode, $A_{2u}^{\mathrm{TO}}(3)$, was predicted to be very small[17] and could not be detected by infrared spectroscopy. This can also be expected

TABLE II. Comparison of experimentally observed A_{2u}^{TO} frequencies in units of cm^{-1} from several sources with the calculated values as obtained from the model I including charge fluctuations and anisotropic dipole fluctuations as discussed in the text. The values in brackets are in THz. For the corresponding displacement patterns see Fig. 9.

Source	$A_{2u}^{\mathrm{TO}}(1)$	$A_{2u}^{\mathrm{TO}}(2)$	$A_{2u}^{\mathrm{TO}}(3)$
Ref. 38	493	248	146
Refs. 17 and 39	500	235	135
Ref. 41	509	243	173
Ref. 18	501	342	242
Ref. 40	494	242	-
Ref. 33	492	347	234
I	482 (14.44)	283 (8.48)	172 (5.15)

TABLE III. Comparison of experimentally observed A_{2u}^{TO} frequencies (Ref. 38) with calculated values in units of cm^{-1} and eigenvectors based on different methods as explained in the text.

Source	ν_{TO}	e^{La}	e^{Cu}	$e^{O_{xy}}$	e^{O_z}
Ref. 17	493.5	−0.07	0.11	−0.45	0.53
Ref. 25	446	−0.09	0.08	−0.42	0.56
Ref. 42	548.5	−0.05	0.03	−0.44	0.55
Ref. 43	847.6	−0.07	0.09	−0.41	0.57
Ref. 26	441	−0.07	0.10	−0.45	0.54
I	482	−0.07	−0.04	−0.35	0.61
Expt. (Ref. 38)	493				
Ref. 17	228.8	0.22	0.26	−0.49	−0.42
Ref. 25	197	0.29	0.04	−0.53	−0.37
Ref. 42	305.4	0.29	0.05	−0.51	−0.39
Ref. 43	370.2	0.18	0.34	−0.51	−0.38
Ref. 26	182	0.21	0.28	−0.50	−0.41
I	283	0.20	0.28	−0.58	−0.30
Expt. (Ref. 38)	248				
Ref. 17	145.2	−0.32	0.87	0.12	−0.03
Ref. 25	119	−0.24	0.93	−0.01	−0.11
Ref. 42	162.5	−0.27	0.92	−0.04	−0.08
Ref. 43	200.3	−0.34	0.85	0.15	0
Ref. 26	132	−0.33	0.87	0.12	−0.02
I	172	−0.33	0.87	0.08	0.04
Expt. (Ref. 38)	146				

from the small LO-TO splitting of this mode in our calculation (see Fig. 9) and is verified by the explicit calculation of the oscillator strengths presented in Sec. III D. So it seems very likely that the experimental groups[18,33] (see Table II) have wrongly assigned the mode with frequency 347 or 342 cm^{-1} to the tetragonal phase, believing that it would be the ''missing'' third A_{2u} mode. It is more likely that the modes around 350 cm^{-1} arise from the orthorhombic distortion of the structure, as is evident from recent neutron measurements[38] and also from infrared spectroscopy.[17] An indication of the ''missing'' A_{2u} mode from infrared data is first reported in Refs. 39 and 41, yielding a frequency of 135 and 173 cm^{-1}, respectively, while the neutron experiment[38] results in 146 cm^{-1}.

From the large size of the calculated LO-TO splitting of the $A_{2u}^{TO}(2)$ mode (see Fig. 9), we correspondingly expect a large oscillator strength, and this mode will dominate the infrared response for polarization along the *c* axis. We will call this mode the ''ferroelectric mode'' (FM) in the following motivated by the fact that in this strong mode the Cu and La cations vibrate against the O_{xy} and O_z anions, and as a consequence the dipole moments generated by the motion of the ions add constructively to a large value. This mode will carry nearly all contributions to the static dielectric constant along the *c* direction. Finally, the B_{2u} mode should be mentioned, which does not induce a dipole moment and so is infrared inactive. As can be seen from Fig. 9 this mode involves only O_x and O_y atoms moving in opposite directions along the *c* axis. The calculated frequency for B_{2u} is in I, 167

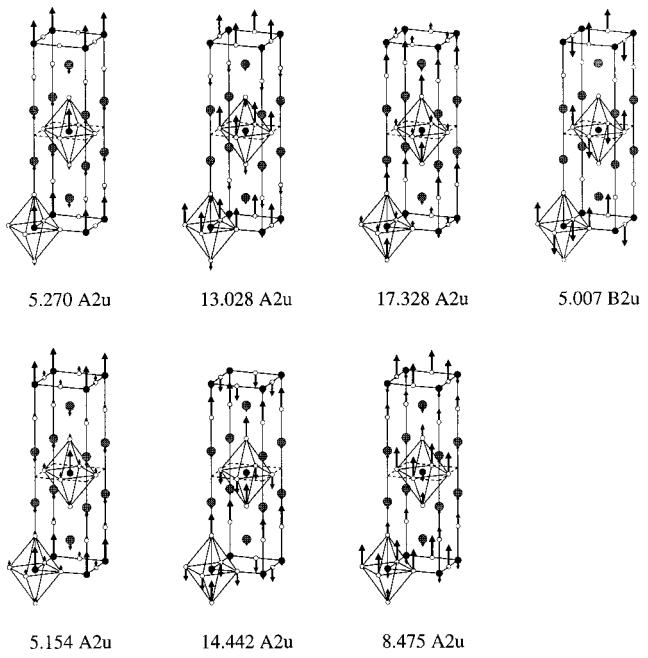

FIG. 9. Displacement patterns of the longitudinal (upper row) and transverse (lower row) A_{2u} modes for tetragonal La_2CuO_4 as calculated with model I. In the upper row additionally the infrared inactive B_{2u} mode is shown. Frequencies are in units of THz.

cm^{-1}, which can be compared to results from LDA, 201 cm^{-1} (Ref. 25), 193 cm^{-1} (Ref. 26).

In order to make a comparison between the calculated eigenvectors and frequencies for the A_{2u} modes as obtained from our calculation with results reported in other theoretical investigations in the field based on different methods, we have collected the corresponding data in Table III. We recognize that there are considerable differences in the calculated frequencies of the A_{2u} modes and thus we have a more or less good agreement of the theoretical values with the neutron experiments.[38] The good agreement of the data cited in Ref. 17 with the experimental results is related to the fact that they are obtained by fitting the neutron results with a shell model. The calculations in Refs. 25 and 26 are based on LDA,[42] on the shell model, and on the potential-induced breathing model.[43] A common feature arises in all calculations, namely, that the eigenvector for the FM points to a large dipole moment and thus to a large oscillator strength in agreement with experiment.

The atomic displacement patterns of the longitudinal and transverse optical E_u modes polarized parallel to the CuO plane as calculated with model I are shown in Fig. 10. From an inspection of the LO-TO splitting it can be supposed that the largest oscillator strength by far is related to the mode with the lowest frequency where the La ion and O_z are sliding in opposite directions parallel to the ions in the CuO plane. The components of the normalized eigenvector for this mode are $[\mathbf{q}\|(1,0,0)]$:

$$\text{TO:}\quad e_y^{Cu}=0.14,\quad e_y^{O_x}=0.02,\quad e_y^{O_y}=0.09,$$

$$e_y^{O_z}=0.64,\quad e_y^{La}=-0.28;$$

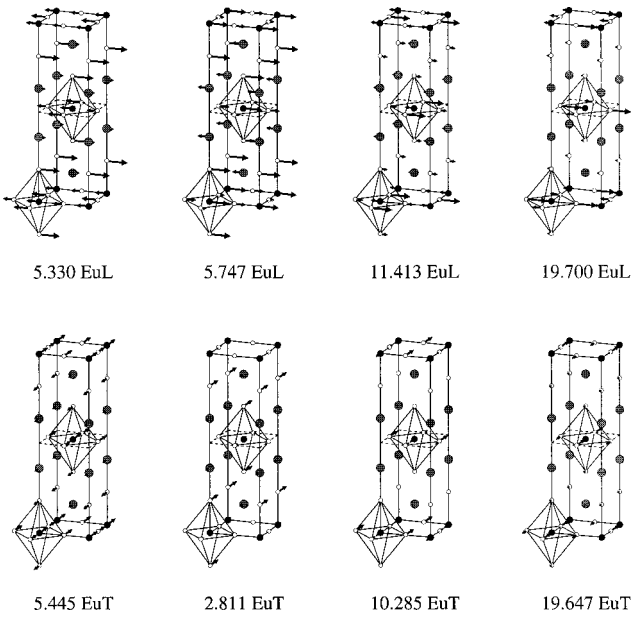

FIG. 10. Displacement patterns of the longitudinal (upper row) and transverse (lower row) E_u modes for tetragonal La_2CuO_4 as obtained from model I. Frequencies are in units of THz.

$$\text{LO:}\quad e_x^{\text{Cu}}=0.63,\quad e_x^{\text{O}_x}=0.17,\quad e_x^{\text{O}_y}=0.05,$$

$$e_x^{\text{O}_z}=0.38,\quad e_x^{\text{La}}=-0.38.$$

An explicit calculation of the oscillator strengths in Sec. III D then shows that this phonon indeed dominates the optical E_u response and the static dielectric constant in the (xy) plane. A comparison of our calculated frequencies for the E_u modes with several experimental sources cited in Ref. 37 is provided in Table IV. As for the A_{2u} modes the agreement is rather satisfying. In Table IV also the calculated results as obtained within the LDA (Refs. 25–27) are listed. As far as the even modes at the Γ point are concerned the experimental data [44] and our calculated values are as follows (the experimental data are specified first):

$$A_{1g}(\text{La}):\ 227\ \text{cm}^{-1},\ 207\ \text{cm}^{-1};$$

$$A_{1g}(\text{O}_z):\ 427\ \text{cm}^{-1},$$

TABLE IV. Comparison of the calculated E_u^{TO} frequencies in the model I with several experimental sources (Ref. 37), and results as obtained in the local-density approximation in units of cm^{-1} using different techniques (Refs. 25–27). See also Fig. 10 for the corresponding displacement patterns. The values in brackets are in TH_z.

Source	$E_u(1)$	$E_u(2)$	$E_u(3)$	$E_u(4)$
	680	350	170	120
Expt. (Ref. 37)	667	358		132
	695	360		145
Ref. 26	630	319	147	22
Ref. 25	650	312	146	75*i*
Ref. 27				39
I	655 (19.65)	343 (10.29)	182 (5.45)	94 (2.81)

$$490\ \text{cm}^{-1}.$$

$$E_g(\text{La}):\ 91\ \text{cm}^{-1},\ 81\ \text{cm}^{-1};$$

$$E_g(\text{O}_z):\ 241\ \text{cm}^{-1},$$

$$251\ \text{cm}^{-1}.$$

D. Dielectric constants, transverse effective charges, and infrared response

The high-frequency ($\hat{\mathbf{q}}$-dependent) macroscopic dielectric constant $\varepsilon_\infty(\hat{q})$ and the elements of the transverse effective charge tensor $\underline{\underline{Z}}_\alpha^T$ are obtained in our approach from Eqs. (11)–(15). For tetragonal La_2CuO_4 only the two independent components $\varepsilon_{\infty,zz}$, $\varepsilon_{\infty,xx}=\varepsilon_{\infty,yy}$ and $Z_{\alpha,zz}^T$, $Z_{\alpha,xx}^T=Z_{\alpha,yy}^T$ must be calculated. The macroscopic dielectric tensor as a function of frequency in the infrared range follows as[45]

$$\underline{\underline{\varepsilon}}(\omega)=\underline{\underline{\varepsilon}}_\infty+\sum_{\sigma=4}^{3s}\frac{\underline{\underline{\Omega}}^2(\sigma)}{\omega^2(\sigma)-\omega^2}\equiv\underline{\underline{\varepsilon}}_\infty+\sum_{\sigma=4}^{3s}\frac{\underline{\underline{S}}(\sigma)\omega^2(\sigma)}{\omega^2(\sigma)-\omega^2}. \tag{18}$$

$\underline{\underline{\varepsilon}}_\infty$ is the high-frequency dielectric tensor and the second term in Eq. (18) describes the contribution from the lattice modes. σ runs over the $3s$-3 optical modes at $\mathbf{q}\equiv\mathbf{0}$ and $\omega(\sigma)$ is the phonon frequency given by the zero-wave-vector dynamical matrix, i.e., without its contribution from the long-ranged effective charge term. The (longitudinal) high-frequency macroscopic dielectric constant $\varepsilon_\infty(\hat{\mathbf{q}})$ and the tensor $\underline{\underline{\varepsilon}}_\infty$ are related in the limit $\mathbf{q}\rightarrow\mathbf{0}$ by

$$\varepsilon_\infty(\hat{q})=\hat{\mathbf{q}}\cdot\underline{\underline{\varepsilon}}_\infty\cdot\hat{\mathbf{q}}. \tag{19}$$

$\underline{\underline{S}}(\sigma)$ in Eq. (18) represents the tensor of the oscillator strength of mode σ. It provides the contribution of that mode to the static dielectric tensor $\underline{\underline{\varepsilon}}(\omega=0)\equiv\underline{\underline{\varepsilon}}_0$. $\underline{\underline{S}}(\sigma)$ is defined as

$$S_{ij}(\sigma)\equiv\frac{\Omega_{ij}^2(\sigma)}{\omega^2(\sigma)}, \tag{20}$$

with

$$\Omega_{ij}^2(\sigma)=\frac{4\pi e^2}{V_z}P_i(\sigma)P_j^*(\sigma) \tag{21}$$

and the electric dipole moments

$$P_i(\sigma)=\sum_{\alpha,j}Z_{\alpha,ij}^T\frac{\tilde{e}_j^\alpha(\sigma)}{\sqrt{M_\alpha}}. \tag{22}$$

Here $\tilde{e}_i^\alpha(\sigma)$ denotes the eigenvector of the zero-wave-vector optical mode, with eigenfrequency $\omega(\sigma)$ and $Z_{\alpha,ij}^T$ is the tensor of the transverse effective charges. In this way the oscillator strengths of the infrared-active phonon modes are connected with the dipole moments arising from the displacements of the ions involved in the vibration. From Table V it can be concluded that especially in model I, where CF's and DF's are allowed, the elements of $\underline{\underline{\varepsilon}}_0$ are much larger than those of $\underline{\underline{\varepsilon}}_\infty$. This means that at low frequencies the optical phonons govern the dielectric behavior. Comparing the result for $\varepsilon_{\infty,xx}$ of model CF (only CF's in the

TABLE V. Calculated matrix elements of the macroscopic high-frequency dielectric tensor $\underline{\underline{\varepsilon}}_\infty$ and the static dielectric tensor $\underline{\underline{\varepsilon}}_0$ for tetragonal La_2CuO_4 together with a corresponding averaged value $\overline{\varepsilon}=\frac{1}{3}(\varepsilon_{xx}+\varepsilon_{yy}+\varepsilon_{zz})$. R2 denotes the *ab initio* rigid-ion model, CF includes additionally charge fluctuations, and CFD (I) is the full model with charge fluctuations and anisotropic dipole fluctuations explained in the text.

	ε_{zz}			$\varepsilon_{xx}=\varepsilon_{yy}$			$\overline{\varepsilon}$		
La_2CuO_4	R2	CF	CFD (I)	R2	CF	CFD (I)	R2	CF	CFD (I)
$\underline{\underline{\varepsilon}}_\infty$	1	1	1.93	1	6.33	6.69	1	4.55	5.11
$\underline{\underline{\varepsilon}}_0$	3.97	3.98	6.86	15.01	20.35	33.20	11.33	14.90	24.42

CuO plane) with that of model I, we see that the screening contribution of the electrons in the CuO plane is mainly due to the CF's. This is different than the situation in the classical ionic crystals, where the DF's are the most influential part.[13] On the other hand, along the *c* axis screening is essentially caused by the DF's along this axis expressing the ionic character between the layers. Possible small contributions by the CF's that could enhance $\varepsilon_{\infty,zz}$ are related to the O_z and La ions. According to the discussion in Sec. III B these contributions, however, can be neglected.

In Table VI the calculated transverse effective charges for the ions in La_2CuO_4 as obtained from model I are listed together with the effective ionic charges of the RIM, Z_α^{ion}. The difference between the two types of charges is a consequence of the corresponding nonrigid electronic polarization process (CF, DF) generated during the displacements of the ions. $Z^T_{\alpha,zz}$ is related to the A_{2u} modes, while $Z^T_{\alpha,xx}=Z^T_{\alpha,yy}$ is apparent in the E_u modes. Finally, from Table VII, where the calculated oscillator strengths of the A_{2u} and E_u modes are shown, we find that the low-frequency optical response is dominated for polarization along the *c* axis by the ''ferroelectric mode'' $A_{2u}^{\text{TO}}(2)$. Here the Cu and La cations vibrate coherently against the O_{xy} and O_z anions (see Fig. 9). For polarization parallel to the CuO plane the strongest mode is the ''sliding mode'' $E_u^{\text{TO}}(4)$ with the lowest frequency (see Fig. 10), where La and O_z are sliding in opposite directions parallel to the Cu and the planar oxygens.

IV. SUMMARY AND CONCLUSIONS

In this paper we have presented a detailed study of the influence of DF's in addition to CF's on the lattice dynamics, the dielectric properties, and the infrared response of HTSC's using La_2CuO_4 as a prototype example. Starting with an *ab initio* RIM with computed effective ionic charges as a reference model to describe the important ionic contribution of binding in the HTSC and the local EPI effects (rigid charge response), we have developed microscopic models for the metallic and the insulating phase, allowing for both CF's and DF's as electronic polarization processes. The calculations of the phonon dispersion and of specific modes are compared with experiments from neutron scattering, infrared spectroscopy, and other theoretical sources.

In the following we summarize our results and conclusions. Taking into account CF's and anisotropic DF's in the electronic density response, a satisfactory agreement with the experimental data of the phonon dispersion of La_2CuO_4 in the metallic and insulating phases is obtained.

From a comparison of different model calculations with the experimental phonon dispersion we can conclude that screening in La_2CuO_4 is best described by a two-dimensional electronic structure in the CuO plane leading to CF's in the plane as the most important process. LDA-based calculations seem to be sufficient for the charge response in the CuO plane in the metallic phase; however, they overestimate the coupling along the *c* axis, i.e., they underestimate the *c*-axis anisotropy. We also find an important contribution of anisotropic screening by DF's where the dipole polarizability dominates along the (ionic) *c* direction. In addition to the nonadiabatic phonons in a small region around the Λ direction in the metallic phase, the main difference between the phonon dispersion in the metallic and insulating phases is the strong softening of the high-frequency Cu-oxygen bond-stretching modes generated by the CF's through the nonlocal EPI. It is very likely that this coupling effect is causing a kink in the electronic dispersion, seen by photoemission.

A possible Peierls instability of the O_B^X mode that is found in other calculations and a renormalization of the quadrupolar mode associated in the literature with a Jahn-Teller electron-phonon interaction both are not supported by our calculations. The behavior of the scissor mode in the RIM points to specific covalent bonding contributions that can be dealt with by off-site CF's. Our calculations also have shown the sensitivity of the tetragonal structure against LTO and LTT tilt arising from direct Coulomb coupling and electronic dipole coupling, respectively.

TABLE VI. Elements of the transverse effective charge tensor $\underline{\underline{Z}}^T_\alpha$ for La_2CuO_4 as calculated with model I. The Z_α^{ion} denote the effective ionic charges of the rigid-ion model as obtained from a tight-binding analysis of the electronic bond structure.

		Z_α^{ion}	$Z^T_{\alpha,zz}$			Z_α^{ion}	$Z^T_{\alpha,xx}=Z^T_{\alpha,yy}$	
I	La	Cu	O_{xy}	O_z	La	Cu	O_{xy}	O_z
Z_α^{ion}	2.28	1.22	−1.42	−1.47	2.28	1.22	−1.42	−1.47
$\underline{\underline{Z}}^T_\alpha$	2.807	0.864	−1.456	−1.783	2.475	1.278	−1.359	−1.625

TABLE VII. Calculated matrix elements for model I and the rigid-ion model R2 of the tensor of oscillator strength $\underline{\underline{S}}(\sigma)$ of La_2CuO_4 for the axial polarized A_{2u} modes and the E_u modes polarized perpendicular to the *c* axis.

	S_{zz}					$S_{xx}=S_{yy}$	
$\underline{\underline{S}}(\sigma)$	$A_{2u}(1)$	$A_{2u}(2)$	$A_{2u}(3)$	$E_u(1)$	$E_u(2)$	$E_u(3)$	$E_u(4)$
I	0.239	4.275	0.416	0.016	0.590	0.029	12.619
R2	0.002	2.779	0.194	0.019	0.527	0.029	6.430

We further have addressed the infrared-active A_{2u} and E_u vibrations and clarified the controversially discussed mode assignment of the former. Moreover, a detailed comparison with other calculations and the experiment has been achieved.

Finally, we have calculated the dielectric properties and the infrared response for a HTSC material in our microscopic approach. Note, that a full *ab initio* calculation for the phonons, the dielectric properties, and the infrared response (transverse effective charges, oscillator strengths) is not available for the insulating phase. From our investigations we find that the low-frequency response is governed in case of A_{2u} symmetry by the ''ferroelectric mode'' and for E_u symmetry by the O_z-La sliding mode with the lowest frequency. Thus, the infrared response along the *c* axis and perpendicular to it, each one of them, is dominated by just one strong phonon reflecting the ionic character of the material along the *c* axis and the ionic layers, respectively. These modes carry nearly all contributions to the components of the static dielectric tensor.

ACKNOWLEDGMENTS

We greatly appreciate the financial support by the Deutsche Forschungsgemeinschaft.

[1] L. Pintschovius and W. Reichardt, in *Neutron Scattering in Layered Copper-Oxide Superconductors*, edited by A. Furrer, Vol. 20 of Physics and Chemistry of Materials with Low Dimensional Structures (Kluwer Academic, Dordrecht, 1998), p. 165.
[2] R. J. McQueeney, Y. Petrov, T. Egami, M. Yethiray, G. Shirane, and Y. Endoh, Phys. Rev. Lett. **82**, 628 (1999).
[3] L. Pintschovius and M. Braden, Phys. Rev. B **60**, R15039 (1999).
[4] A. P. Litvinchuk, C. Thomsen, and M. Cardona, in *Physical Properties of High Temperature Superconductors IV*, edited by D. M. Ginsberg (World Scientific, Singapore, 1994), p. 370.
[5] A. Lanzara, P. V. Bogdanov, X. J. Zhou, S. A. Kellar, D. L. Feng, E. D. Lu, T. Yoshida, H. Eisaki, A. Fujimori, K. Kishio, J.-I. Shimoyama, T. Noda, S. Uchida, Z. Hussain, and Z.-X. Shen, Nature (London) **412**, 510 (2001).
[6] R. J. McQueeney, J. L. Sarrav, P. G. Pagliuso, P. W. Stephens, and R. Osborn, Phys. Rev. Lett. **87**, 077001 (2001).
[7] H. Krakauer, W. E. Pickett, and R. E. Cohen, Phys. Rev. B **47**, 1002 (1993).
[8] C. Falter, M. Klenner, and W. Ludwig, Phys. Rev. B **47**, 5390 (1993).
[9] C. Falter, M. Klenner, and Q. Chen, Phys. Rev. B **48**, 16 690 (1993).
[10] C. Falter, M. Klenner, G. A. Hoffmann, and Q. Chen, Phys. Rev. B **55**, 3308 (1997).
[11] C. Falter and G. A. Hoffmann, Phys. Rev. B **61**, 14 537 (2000).
[12] C. Falter, M. Klenner, and G. A. Hoffmann, Phys. Rev. B **57**, 14 444 (1998).
[13] C. Falter, M. Klenner, G. A. Hoffmann, and F. Schnetgöke, Phys. Rev. B **60**, 12 051 (1999).
[14] C. Falter and G. A. Hoffmann, Phys. Rev. B **64**, 054516 (2001).
[15] P. B. Allen, Phys. Rev. B **16**, 5139 (1977).
[16] L. Pintschovius and W. Reichardt, in *Physical Properties of High Temperature Superconductors IV*, edited by D. M. Ginsberg (World Scientific, Singapore, 1994), p. 295.
[17] R. Henn, J. Kircher, and M. Cardona, Physica C **269**, 99 (1996).
[18] R. T. Collins, Z. Schlesinger, G. V. Chandrashekhar, and M. W. Shafer, Phys. Rev. B **39**, 2251 (1989).
[19] G. D. Mahan, Phys. Rev. A **22**, 1780 (1980).
[20] G. D. Mahan and K. R. Subbaswamy, *Local Density Theory of Polarizability* (Plenum, New York, 1990).
[21] C. Falter, M. Klenner, and G. A. Hoffmann, Phys. Rev. B **52**, 3702 (1995).
[22] H. Krakauer, W. E. Pickett, and R. E. Cohen, J. Supercond. **1**, 111 (1988).
[23] M. Klenner, C. Falter, and Q. Chen, Ann. Phys. (Leipzig) **3**, 225 (1994).
[24] J. M. Longo and P. M. Racah, J. Solid State Chem. **6**, 526 (1973).
[25] D. J. Singh, Solid State Commun. **98**, 575 (1996).
[26] Cheng-Zhang Wang, Rici Yu, and H. Krakauer, Phys. Rev. B **59**, 9278 (1999).
[27] R. E. Cohen, W. E. Pickett, and H. Krakauer, Phys. Rev. Lett. **62**, 831 (1989).
[28] M. K. Crawford, M. N. Kunchur, W. E. Farneth, E. M. McCarron III, and S. J. Poon, Phys. Rev. B **41**, 282 (1990).
[29] J. P. Frank, S. Harker, and J. H. Brewer, Phys. Rev. Lett. **71**, 283 (1993).
[30] W. Weber, Phys. Rev. Lett. **58**, 1371 (1987).
[31] D. V. Fil, O. I. Tokar, A. L. Shelankov, and W. Weber, Phys. Rev. B **45**, 5633 (1992).
[32] S. Uchida, T. Ido, H. Takagi, T. Arima, Y. Tokura, and S. Tajima, Phys. Rev. B **43**, 7942 (1991).
[33] S. Uchida, K. Tamasaku, and S. Tajima, Phys. Rev. B **53**, 14 558 (1996).
[34] M. J. de Weert, D. A. Papaconstantopoulos, and W. E. Pickett, Phys. Rev. B **39**, 4235 (1989).
[35] C. Falter, M. Klenner, and G. A. Hoffmann, Phys. Status Solidi B **209**, 235 (1998).
[36] J. D. Axe, A. H. Moudden, D. Hohlwein, D. E. Cox, K. M. Mohanty, A. R. Moodenbough, and Youwen Xu, Phys. Rev. Lett. **62**, 2751 (1989).
[37] J. Humlíček, R. Henn, and M. Cardona, Phys. Rev. B **61**, 14 554 (2000).

[38] S. L. Chaplot, W. Reichardt, and L. Pintschovius, Physica B **219–220**, 219 (1996).
[39] R. Henn, A. Wittlin, M. Cardona, and S. Uchida, Phys. Rev. B **56**, 6295 (1997).
[40] J. H. Kim, H. S. Somal, M. T. Czyzyk, D. van der Marel, A. Wittlin, A. M. Gerrits, V. H. M. Duijn, N. T. Hien, and A. A. Menovsky, Physica C **247**, 297 (1995).
[41] A. V. Bazhenov, C. B. Rezchikov, and I. S. Smirnova, Physica C **273**, 9 (1996).
[42] J. Prade, A. D. Kulkarni, F. D. de Wette, W. Kress, M. Cardona, R. Reiger, and U. Schröder, Solid State Commun. **64**, 1267 (1987).
[43] R. E. Cohen, W. E. Pickett, H. Krakauer, and L. L. Boyer, Physica B **150**, 61 (1988).
[44] L. Pintschovius, N. Pyka, W. Reichardt, A. Yu. Rumiantsev, M. L. Mitrofanov, A. S. Ivanov, G. Collin, and P. Bourges, Physica C **185–189**, 156 (1991).
[45] L. J. Sham, Phys. Rev. **188**, 1431 (1969).